Computers and Geotechnics

Volume 103, November 2018, Pages 201-217

https://doi.org/10.1016/j.compgeo.2018.07.014

Impact forces of granular flows on rigid structures: Comparison between discontinuous (DEM) and continuous (MPM) numerical approaches

Francesca Ceccato[a], Irene Redaelli[b], Claudio di Prisco[b], Paolo Simonini[a]

[a]DICEA – University of Padua, via Ognissanti 39, 35129 Padua, Italy
[b]DICA – Politecnico di Milano, Pz. L. da Vinci 32, 20133 Milano, Italy

Abstract: The evaluation of forces due to the impact of flow-slides against structures is essential for both risk assessment and protection structure design. However, the impact process is very complex and not fully understood yet. Peak forces are in fact commonly evaluated by simplified empirical methods whose reliability is questionable. In this paper, the impact process is numerically investigated by comparing the results obtained from software based on a discontinuous Discrete Element Method (DEM) and a continuous Material Point Method (MPM). The impact process and its key features are highlighted and the principal parameters influencing the peak force value are identified. This study focuses on the impact phase, rather than on the propagation phase. The soil mass is initially positioned in front of the wall with a prescribed uniform velocity and the evolution of the impact force is monitored.

Edited version of the paper can be downloaded at: https://www.sciencedirect.com/science/article/pii/S0266352X18301903

1 Introduction

Landslides of the flow type, i.e. when the material behaves like a fluid and can move with high velocities, are among the most destructive landslide events. They include a wide range of phenomena, still difficult to classify, because they present mixtures of water, air and solid grains with percentages extremely variable in space and time. Examples of flow-like landslides are rock avalanches, dry sand/debris flow, sand flowslides, debris flows, sensitive clay flowslides and mud flows [1].

To reduce the risk associated with these class of landslides, very common protection measures are earth embankments and rigid obstacles built with the purpose of deviating or stopping the flow. To design these sheltering structures, the maximum impact force is often estimated by means of simplified relationships which

are based on theories that consider the granular material to be an incompressible fluid and evaluate the fluid force according to either the hydrostatic or hydrodynamic approaches. The former approach assumes a triangular distribution of the normal pressure, whose maximum value is the hydrostatic pressure multiplied by an empirical factor ($p_{max}=k\rho gh$, ρ=bulk density, h=flow thickness, g=gravity acceleration, k=empirical factor) [2,3]. The latter assumes a constant pressure distribution along depth, in which the pressure is a modified value of the dynamic pressure ($p_{max}=a\rho v_0^2$, v_0=impact velocity, a=empirical factor) [4,5]. The empirical factors *a* and *k* have been estimated with both small and large scale test results and are a function of the flow characteristics. These coefficients vary within a wide range, making the practical use of these approaches rather difficult. More recently, mixed approaches, in which the peak pressure is a function of both velocity and thickness, have also been proposed [6,7].

In the past, the maximum impact force rarely has been assessed by using numerical codes. In fact, only very recently, computational tools able to deal with large displacements and to simulate soil-structure interaction increased in popularity. The aim of this paper is to study the impact process numerically, thus contributing to a better understanding of the phenomenon. This will lead to a better estimation of the maximum impact force and, therefore, a more efficient design of protective structures with respect to traditional methods.

Numerical techniques suitable for the study of impact forces are Discrete Element Methods (DEMs), Eulerian methods, Arbitrary Lagrangian-Eulerian (ALE) methods, and Lagrangian particle-based methods. DEMs apply a discrete approach in which the granular material is represented by an assembly of particles moving independently and interacting at contact points [8]. They can simulate the granular material response, both under static and dynamic conditions [9–11], by taking into consideration the microstructural response of the material without introducing sophisticated constitutive models. They are also capable of automatically taking into account large displacements [12–15]. Nevertheless, the computational cost may become excessive when the whole landslide process is simulated [16].

On the other hand, Eulerian methods [17], ALE [18,19], and Lagrangian particle-based methods such as SPH, PFEM, FEMLIP, and MPM [20–25] apply a continuum approach. Choosing a suitable constitutive model is a key issue for the study of flow-like landslides by means of continuum approaches. The debate around the most appropriate constitutive equation for describing geophysical flows is still active [26,27]. Part of the scientific community uses soil-mechanics concepts (elastoplasticity) [25,26,28], while another part prefers viscoplastic models [29,30] and still others provide phenomenological constitutive equations merging solid and fluid mechanics concepts [31] or physically based constitutive models [32–35].

In this paper, we will study the impact of a dry granular mass on a rigid barrier by employing both the Discrete approach (DEM) and the continuum approach by using the Material Point Method (MPM) [36] in which

an elastic-perfectly plastic constitutive model with Mohr-Coulomb failure criterion is implemented. The obstacle is assumed to be rigid in order to both generalize the numerical results and to maximize the impact force. This is a standard approach where the deformability of the impacting object is extremely larger than the deformation of the obstacle.

The DEM numerical campaign has been performed using the three-dimensional code PFC3D 4.0, which has been largely employed to simulate both dry granular flows [37,38] and landslide impact processes [12,39].

The MPM code used in this study (Anura3D) was developed to solve 3D dynamic large deformation problems in geotechnical and hydromechanical engineering and was extensively validated for quasi-static and dynamic problems in geomechanics [40–42]. In the past decade, this code was successfully used in a large number of applications such as landslides [43,44], soil penetration problems [45–48], soil erosion and sedimentation [49,50].

In the following, only the impact phenomenon is considered; the granular impacting mass is placed in front of the rigid barrier with a predefined density and velocity.

The two numerical methods will be employed to quantitatively estimate the impact force on the wall and to analyze the effect of impact velocity, inclination of the flow front and the macromechanical and micromechanical material parameters.

This paper critically discusses the differences between the results obtained by using the two methods, highlighting the limitations of the continuum approach due to the choice of the elasto-plastic constitutive relationship.

In Section 2, the DEM and MPM models are briefly presented. A correlation between the macroscopic input parameters of the continuum model and the microscopic input parameters of the discrete model is established based on 1D confined flow benchmark tests. In Sections 3 and 4 the essential features of the impact process are discusses, emphasizing the effect on the impact force of initial velocity, front inclination and porosity/elastic modulus in DEM/MPM simulations. Concluding remarks are in Section 5.

2 Models

This study considers the impact of a prismatic mass of length L=15m, height h=3m, on a 6m-high vertical rigid wall. The flow is assumed to slide on a horizontal frictional sliding plane. Plane strain conditions are imposed by confining the soil mass between two smooth lateral boundaries.

In natural granular flows, the shape of the front is related to numerous factors such as the slope inclination, the coefficient of lateral soil mass spreading, the average velocity of the sliding mass, the overall friction angle and the density of the soil mass [51–53]. These aspects are not considered in this paper, which disregards the propagation phase, and the front of the landslide mass is assumed to be planar and inclined at an angle α.

At the initial instant of time, corresponding to the time just before the impact, an initial uniform velocity v_0 is assigned to the mass. A parametric study has been performed to assess the influence of v_0 and α (Sec. 4).

The evolution of the impact force on the wall is monitored and the results are normalized with respect to the model width.

The DEM and MPM models are represented in Figures 1 and 2, respectively. The following sections report the details relative to the DEM and MPM models separately.

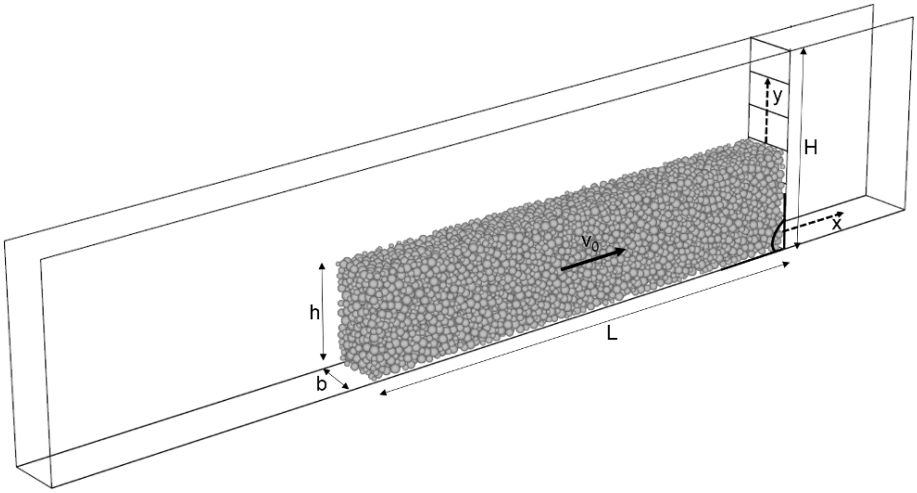

Figure 1 Geometry and discretization of the DEM model

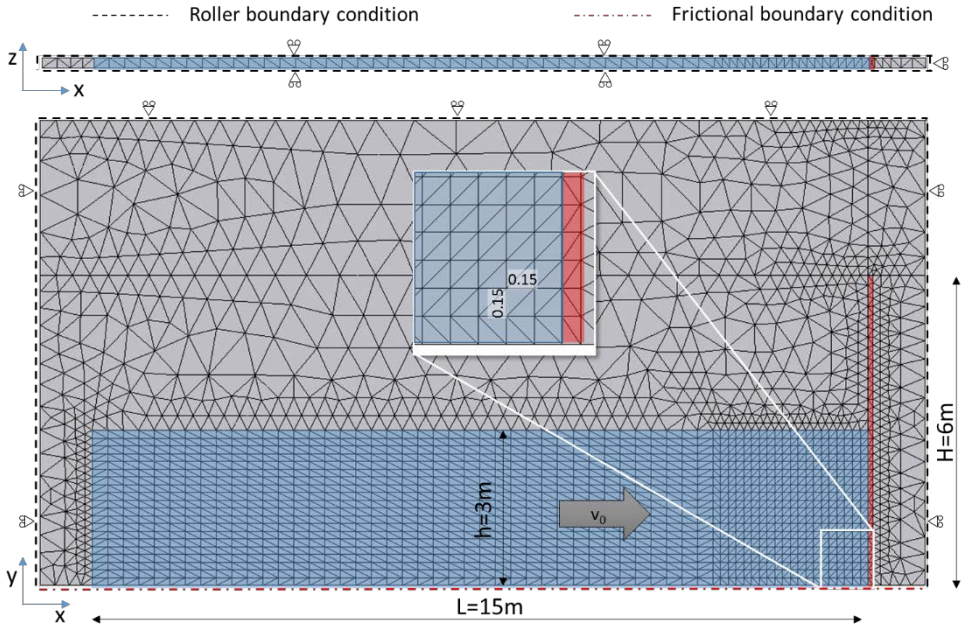

Figure 2 Geometry and discretization of the MPM model, xz plan view (top) and xy side view (bottom) of the 3D model.

2.1 DEM model

The soil mass is represented by an assembly of polydisperse spherical particles of density ρ_s. The grain size distribution is uniform and it is generated by specifying the average grain diameter D and the ratio between the maximum and minimum diameter D_{max}/D_{min}. Before the impact, the mass is characterized by an initial porosity *n*. The reference bulk density of the dry grain assembly is $\rho = (1-n)\rho_s = 1430 kg/m^3$ which has been obtained with the reference porosity *n*=0.45 and the reference grain density ρ_s=2600kg/m^3. Typical values of ρ_s in real rock avalanches are between 2500 and 2800kg/m^3, while the porosity can vary between 0.3 (very dense) to more than 0.5 [54], thus the assumed value of bulk density is considered representative of field conditions.

A parametric analysis has been performed to assess the influence of the initial mass porosity *n* on the impact phenomenon (Sec. 4.3). As explained in Sec. 2.2, the impact pressure depends on the impact velocity (v_0), the speed of the compression wave (c) on the material and the bulk density (ρ); in order to investigate the effect of the porosity keeping a constant bulk density, when changing the material porosity, the density of the grains is scaled.

The mass is confined between two vertical frictionless walls. The authors have performed a sensitivity analysis to assess the influence of the model width (b) on the numerical results. The minimum value for the width not affecting the numerical results was obtained equal to 8D [12].

Grain contacts are governed by a linear force-displacement law in conjunction with Coulomb's friction law; the normal and tangential stiffnesses k_n/D and k_s/D and the interparticle friction angle φ_s are taken from [12,55]. In order to quantitatively reproduce the real soil response, where particles have an irregular shape, particle rotation has been inhibited [55]. In any case, for the problem here analyzed, where most of the mass experiences collisions among grains instead of permanent force chains, this hypothesis does not play any quantitative role. The authors performed some analyses not inhibiting grain rotations and observed that the differences in the value of the maximum impact force are quantitatively negligible (see Appendix A).

No numerical damping is used in the simulations. The time-step Δt has be chosen in order to guarantee the numerical stability of the explicit integration algorithm [56] and it is equal to $\Delta t = \delta\sqrt{m/k_n}$, where m is the particle mass ($m = 1/6\rho_s D^3$) and δ is a reduction factor equal to 0.8. The micro-mechanical parameters adopted in the DEM simulation are reported in Tab. 1.

Table 1 Micro-mechanical parameters of DEM simulations

Average grain diameter (D) [m]	0.2
Ratio between maximum and minimum diameter (D_{max}/D_{min}) [-]	1.4
Particle density (ρ_s) [kg/m^3]	2600
Normal particle stiffness (k_n/D) [MPa]	300

Shear particle stiffness (k_s/D) [MPa]	75
Interparticle friction angle (φ_s) [°]	17
Interface particle-base friction angle (φ_b) [°]	17
Interface particle-wall friction angle (φ_w) [°]	31

The modelling procedure consists in the following stages:

1. Generation of the granular mass by assigning an initial porosity and the prescribed uniform granular size distribution;
2. Relaxation of the assembly under zero gravity. At the end of this stage the mass is free from spurious contact forces;
3. The initial velocity, interparticle friction and gravity are assigned to the whole assembly;
4. The impact is simulated and the evolution of the horizontal impact force on the assembly is monitored over time.

Sensitivity analyses are performed to investigate the influence of D, φ_s, and the friction angles between grains and base (φ_b) and between grains and wall (φ_w), with reference to n=0.45 (see Appendix A). These analyses showed that the average grain diameter D (i.e. the number of particles) does not seem to affect the numerical results; indeed, only a small discrepancy is observed in the initial value of the impact force due to the interaction between the first layer of particles and the obstacle. The influence of φ_s and φ_w on the maximum impact force is negligible. Whereas the particle-base friction φ_b modifies the value of the maximum impact force in case of inclined fronts.

2.2 MPM model

In the MPM model, the contact algorithm originally proposed in [57] is used to simulate the frictional contact at the sliding base of the soil mass (φ_b=17°) and at the obstacle (φ_w=31°). Roller boundary conditions are applied at the remaining surfaces.

Initially, the vertical stress increases linearly with depth ($\sigma_{v0} = \gamma h_s$ γ=soil unit weight and h_s=depth of the considered point from the free surface) and the horizontal stress σ_{h0} is proportional to the vertical stress through the coefficient $K = \frac{\sigma_{h0}}{\sigma_{v0}} = 0.40$.

In MPM, the results are sensitive to the mesh refinement and number of material points (MPs) per element. The mesh is finer in the vicinity of the wall, where larger gradients of stress and strain are expected. In case α=90°, a structured mesh discretizes the soil mass and each cubical unit is divided into 6 tetrahedral elements (Fig. 2). The considered problem is essentially bidimensional; however, only 3D simulations are currently allowed with the used code. The width of the model is kept constant and equal to 0.20m; only one column of elements

is used along this direction. For inclined fronts, an unstructured mesh with an element size similar to the α=90° case is used.

The sensitivity analyses presented in Appendix B have been performed to determine the optimal discretization and to investigate the effects of K, φ_b and φ_w. These simulations showed that, for the considered range of input parameters, the influence of the initial horizontal stress is negligible. The interface friction angle slightly modifies the results for inclined fronts, but are irrelevant for the maximum impact force in case α=90°.

In this paper, the constitutive behavior of the material is modelled by means of a linear elastic perfectly plastic model with Mohr-Coulomb failure criterion [58]. The input parameters are the Young modulus (E), the Poisson's ratio (ν), the internal friction angle (φ), the dilatancy angle (ψ) and the cohesion (c'). Since the aim of this paper consists in quantitatively comparing MPM and DEM results, a fundamental issue concerns the calibration of the constitutive parameters for the MPM model. The strategy followed by the authors is to keep fixed the micro-mechanical parameters used in the DEM analyses and to obtain the equivalent macro-mechanical constitutive parameters for the constitutive relationship used in the MPM code.

For the Mohr-Coulomb plastic surface, a friction angle equal to 37° is employed; this value has been evaluated as a function of the DEM interparticle friction angle φ_s by means of the following relationship, numerically obtained by fitting DEM results by [59]:

$$\varphi = 1.5\varphi_s + 11.5 \quad (1)$$

Sensitivity analyses reported in Appendix B demonstrated that the material friction angle does not significantly influence the impact force. Both the cohesion (c') and the dilatancy angle (ψ) are imposed equal to zero. Since dilatancy is assumed nil, i.e the material is supposed to behave at the critical state, the volumetric compaction is purely elastic.

The choice of the elastic parameters is not straightforward. Nevertheless, as it is commonly assumed in geomechanics, the value of the Poisson ratio employed here in the following is equal to 0.2. In order to quantitatively compare the DEM and MPM results, the Young modulus has been calibrated on the basis of the DEM response as follows.

The impact of a material with porosity n=0.45 under confined conditions is considered (Fig. 3). In this case, vertical fixities are applied at the top boundary of the flow. The initial velocity is v_0=8.8m/s and the flow front is vertical (α=90°). When the granular flow hits the obstacle, it is forced to be compressed; a compression shock wave is generated, and it propagates upstream.

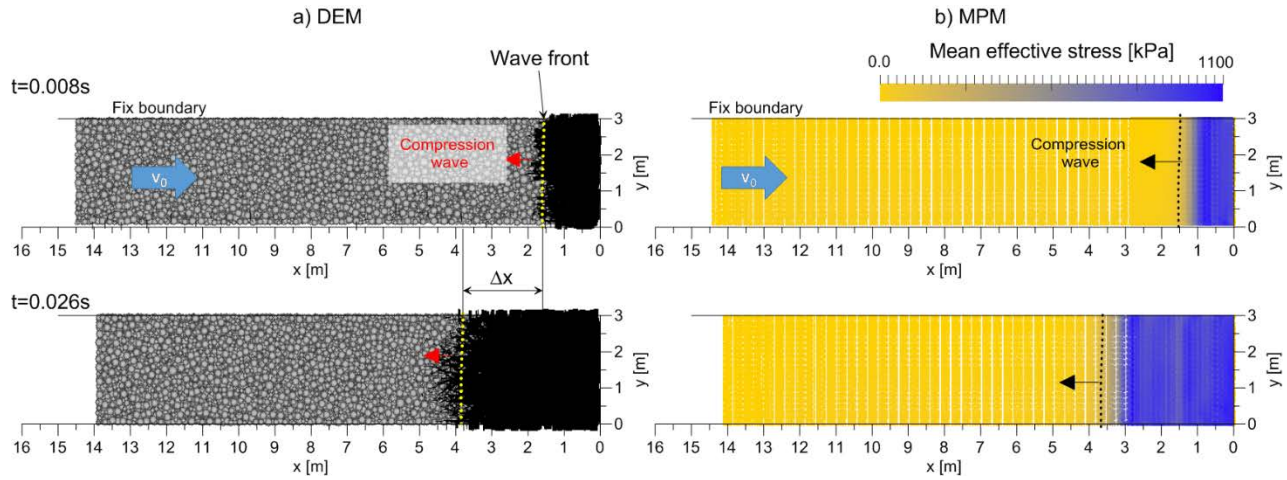

Figure 3 Generation and propagation of compression wave during the impact in confined conditions (material 1, α=90°, v_0=8.8m/s). Comparison between DEM and MPM numerical results.

According to the principle of linear impulse [60], in a homogeneous and elastic medium, the maximum impact pressure is mainly a function of the celerity of the shock wave c. Indeed, the dynamic peak pressure is

$$p = \rho c v_0 \qquad (2)$$

where *c* is close to the sound speed, depending on both the confined elastic modulus ($E_c = E(1-\nu)/((1+\nu)(1-2\nu))$) and the material density:

$$c = \sqrt{E_c/\rho} \qquad (3)$$

In DEM, because of the particulate nature of the material, the shock wave necessarily causes an irreversible compaction of the mass. For this reason, the wave propagating within the medium cannot be considered to be ideally elastic. The celerity of the propagation wave is primarily a function of the porosity (n), but also the normal and tangential stiffness (k_n/D, k_s/D), and the velocity of the impacting mass (v_0) play a role. In this paper, the value of c is estimated for different values of the porosity, while keeping v_0=8.8 m/s, k_n/D=300MPa, and k_s/D=75MPa (Tab. 1). The grain density is scaled with the porosity in order to keep a constant total mass and bulk density.

The first instants of the impact are considered and the position of the wave front is evaluated by analyzing the distributions of the force chains developing within the soil mass (Fig. 3a). From the simple relation $c = \Delta x/\Delta t$, where Δx is the displacement of the wave front in the time interval Δt, the celerity of the compression wave is calculated and the elastic modulus is thus estimated with Eq. 3.

By means of this procedure, we obtained the values of E for different porosities (Tab. 2). These parameters allow a good agreement between MPM and DEM in terms of wave propagation as shown in Fig. 3 for the case n=0.45.

The material parameters used for MPM simulations, for different values of porosity, are summarized in Tab. 2.

Table 2 Material parameters of MPM simulations

Material ID	1	2	3	4	5
Porosity (n) [-]	0.45	0.50	0.55	0.60	0.65
Bulk density (ρ) [kg/m^3]	1430	1430	1430	1430	1430
Young modulus (E) [kPa]	24000	10000	2000	1000	600
Poisson ratio (ν) [-]	0.2	0.2	0.2	0.2	0.2
Celerity of compression wave (c) [m/s]	137	88	40	28	22
Friction angle (φ) [°]	37	37	37	37	37

3 Analysis of the impact process (free surface)

In this section, by using the parameters of Tab. 1 and 2 (material 1), the impact process will be studied and the DEM and MPM numerical results will be compared in two cases: (i) unconfined flow and vertical front, (ii) unconfined flow and inclined front (α=60°).

In a free-surface granular flow the impact force is characterized by an early and very high peak and subsequently decreases to zero (Fig. 4a-b). The rapid decrease in the force value with time, numerically reproduced by both approaches, can be justified by analyzing the screenshots in Fig. 4c-l, where the force chains and the mean effective stress are reported for DEM and MPM numerical analyses, respectively. A compression shock wave develops when the material hits the obstacle, but the lack of confinement generates a rarefaction wave that propagates downward causing a progressive decrease in the mean effective stress. The positions of the front of the compression and rarefaction waves can be recognized by the intensity of the force chains and the magnitude of the mean effective stress and they are highlighted by the dotted lines in Fig. 4c-l.

In brief, the sudden reduction in the value of the impact force with time is strictly related to the bi-dimensionality of the problem and, for this reason, is totally absent in the case of confined impact.

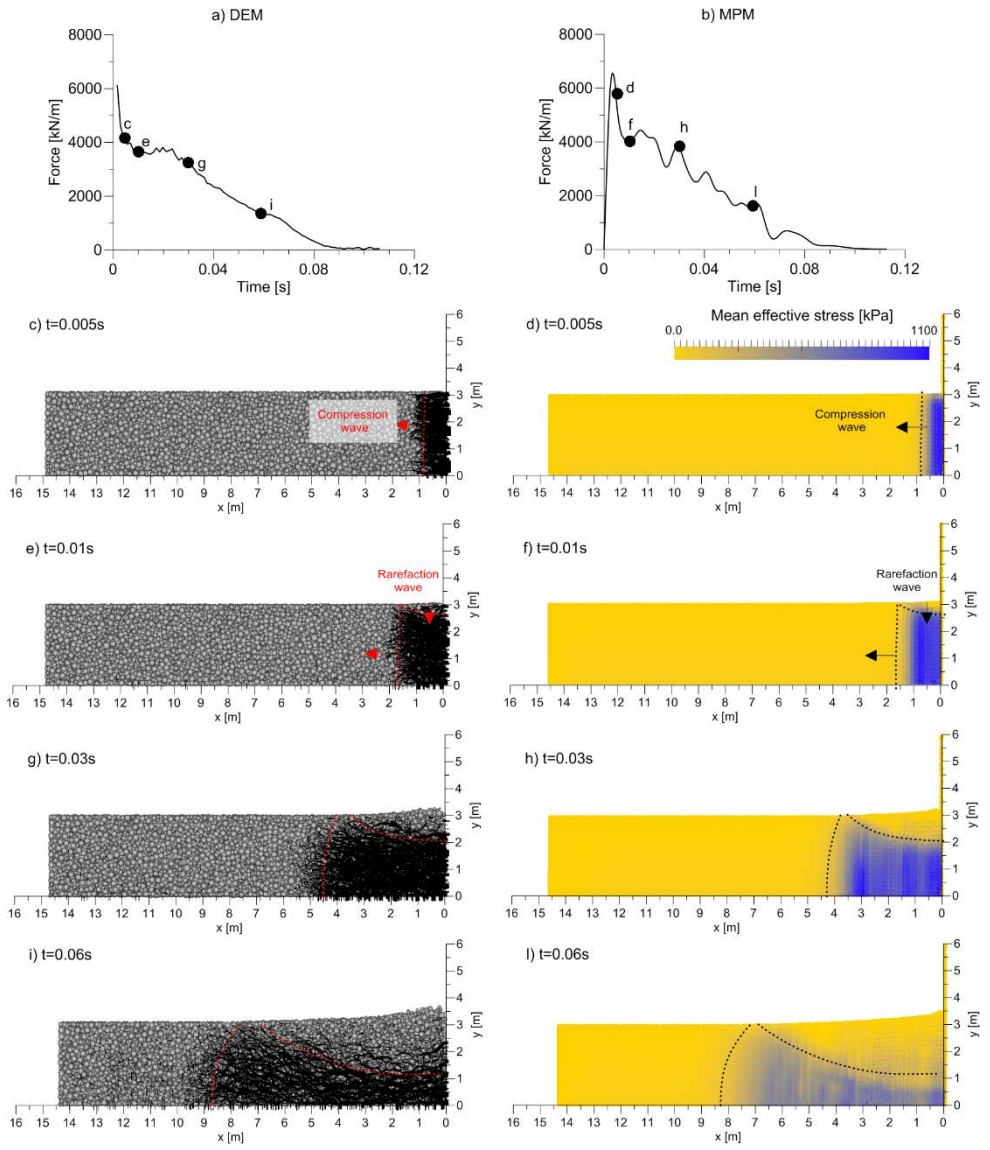

Figure 4 Generation and propagation of compression/rarefaction waves during the impact (material 1, α=90°, v_0=8.8m/s). Comparison between DEM (left) and MPM (right) numerical results. Full dots in subfig. a-b indicate the point to which subfig. c-l are referred.

When the front is not vertical (Fig. 5, α=60°), the force increases with a slower rate and the value of the maximum impact force is significantly lower compared to the case of vertical front (Fig. 5a-b). As confirmed by the screenshots plotted in Fig. 5c-l, in this case the impact process is more complex and, in addition to the interactions between compression and rarefaction waves, the shape of the flow boundary near the wall changes with time, thus the contact area between the mass and the obstacle increases in time, causing the observed slower increment of the impact force. As it was already discussed in [61], the geometry of the front, even if commonly disregarded, drammaticaly affects the value of the maximum impact force.

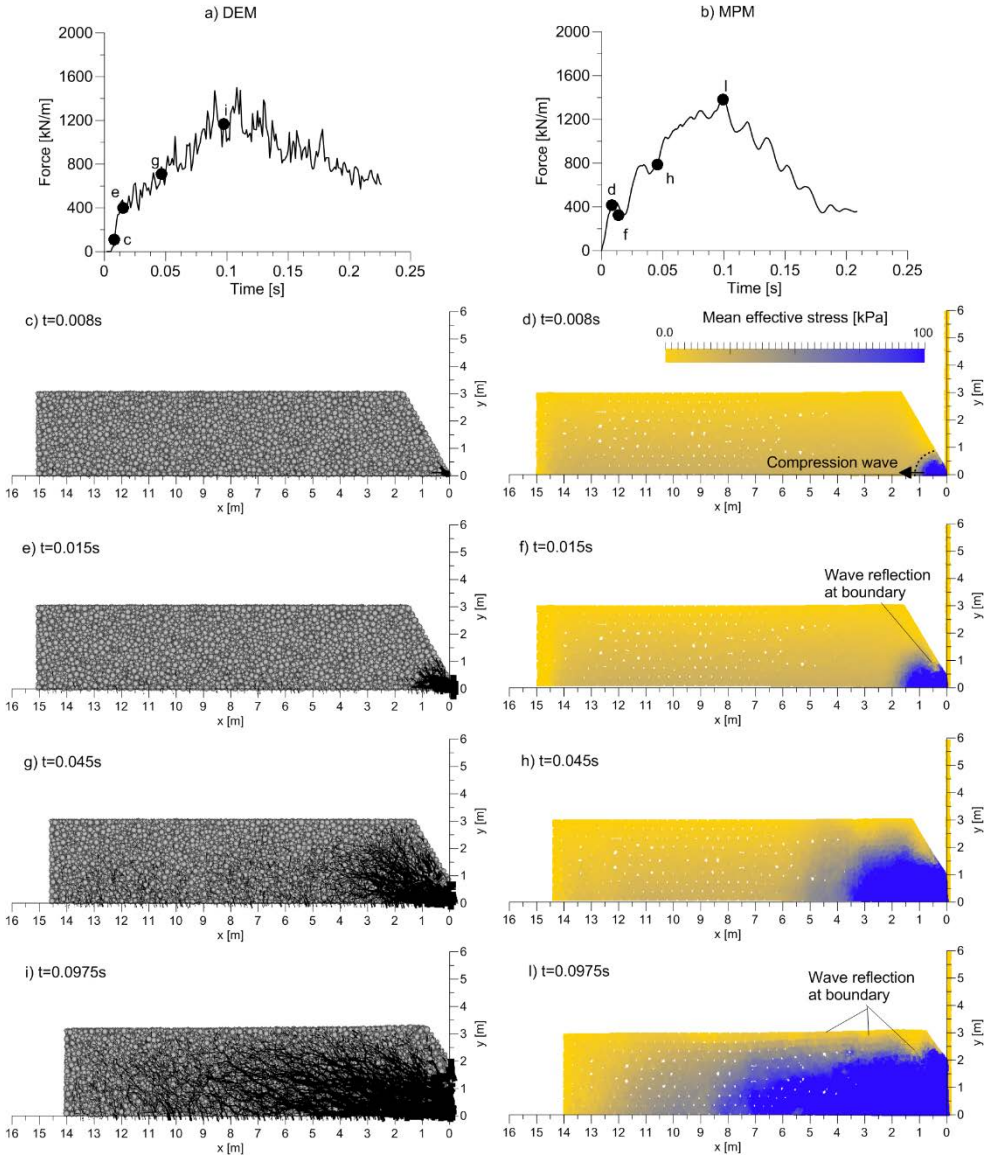

Figure 5 Generation and propagation of compression/rarefaction waves during the impact: DEM (left) and MPM (right) numerical results (material 1, α=60°, v=8.8m/s). Full dots in subfig. a-b indicate the point to which subfig. c-l are referred.

4 Parametric analysis

The evolution of impact force and its peak value (F_{max}) depends on the material's properties, the geometrical and kinematical features of the flow, and the characteristic of the structure. In this section, the effect of impact velocity, flow front inclination and porosity/Young modulus on the force exerted on the vertical wall are analyzed. The material parameters for the MPM simulations are listed in Tab. 2 and they have been derived with the procedure explained in Sec. 2.

4.1 Effect of impact velocity

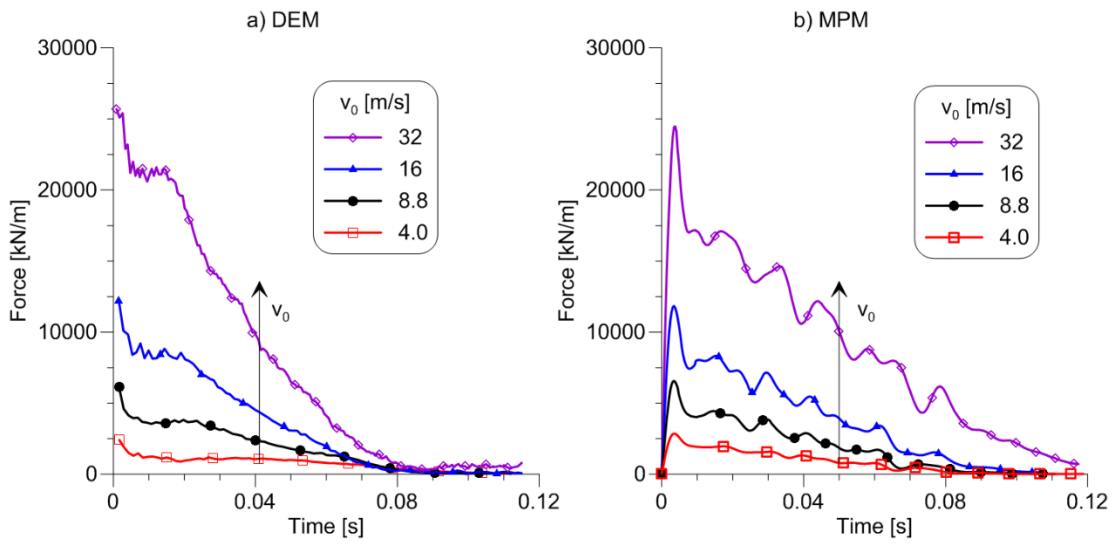

Figure 6 Impact force evolution over time for different impact velocities: DEM (a) and MPM (b) numerical results (material 1, α=90°)

In Fig. 6, the force-time curves for α=90°, material 1 (Tab. 2), and different impact velocities are reported for the DEM and MPM models. The quantitative and qualitative agreement between the results is evident. In both methods, the higher the impact velocity, the higher the maximum impact force. The shape of the force-time curve is not affected by the impact velocity: the force rapidly reaches a peak and then decreases to zero in about 0.09s.

There is a good agreement between the value of the maximum impact force obtained numerically and calculated with the theory of linear impulse (Eq. 2), especially for the reference velocity (8.8m/s), but for different initial velocities, the scatter between DEM and the theoretical solution slightly increases (Tab. 3). This is due to the hypothesis of assuming a constant value of celerity c, independently of the initial velocity of the mass, employed to obtain the elastic modulus in Eq. 3.

Table 3 Maximum impact force as function of velocity for different methods.

v_0 [m/s]	F_{max} [kN/m]		
	Theory (Eq. 2)	DEM	MPM
4	2597	2410	2853
8,8	5409	6120	6564
16	9627	12200	11840
32	19001	26562	24480

4.2 Effect of front inclination

In Fig. 7, the different force-time curves obtained by employing the DEM and MPM methods for v_0=8.8m/s, material 1 and different values of the front inclination α are reported. Again, a good agreement between MPM and DEM results can be appreciated.

A decreasing front inclination results in both longer durations and decreasing values of the maximum impact force. This is due to the geometry of the flow boundary. On one hand, the pressure on the obstacle is smaller because it is influenced by the rarefaction waves generated at the boundary (see Sec. 3); on the other hand, the peak force depends not only on the pressure, but also on the height of the flow in contact with the obstacle, which increases over time for non-vertical fronts. The screenshots plotted in Fig. 8, corresponding to the instant of time in which the peaks in Fig. 7a and 7b are reached, highlight how at the peak time, the height of the material in contact with the obstacle (h_{peak}) is lower than the reference flow height (h).

The relationship between F_{max} and v_0 is linear in case α=90° (Fig. 9). This is in agreement with the theory of linear impulse but in contrast with the hydrodynamic theory that assumes a quadratic relation ($F \propto \rho v_0^2$). In case of non-vertical fronts, this linearity is lost because of the previously discussed geometrical effects (Fig. 9). The peak force and the impact velocity seem to be related by a quadratic function.

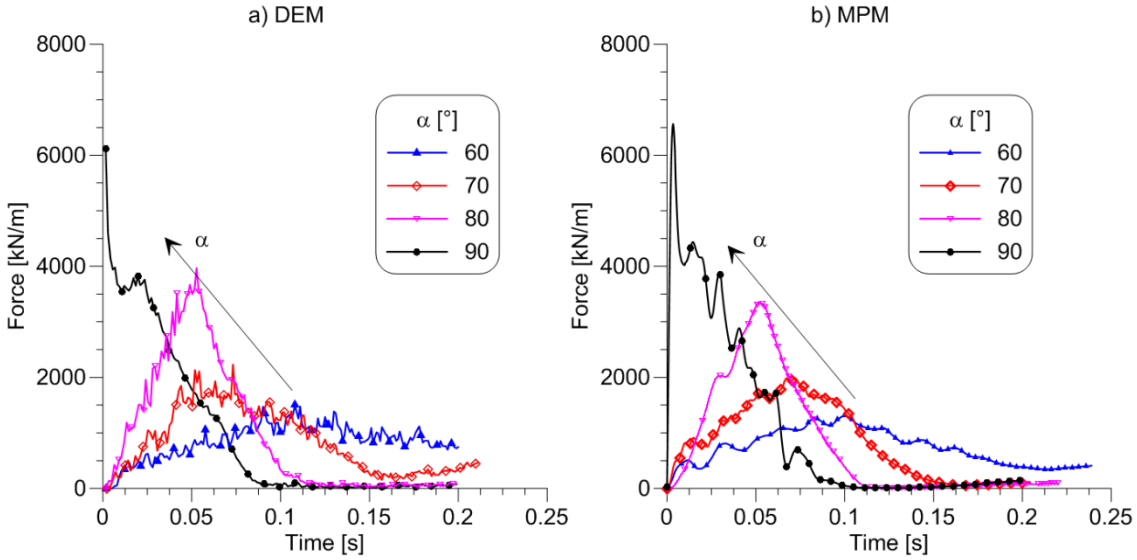

Figure 7 Impact force evolution with time for different front inclinations: DEM (a) and MPM (b) numerical results (n=0.45, v=8.8m/s)

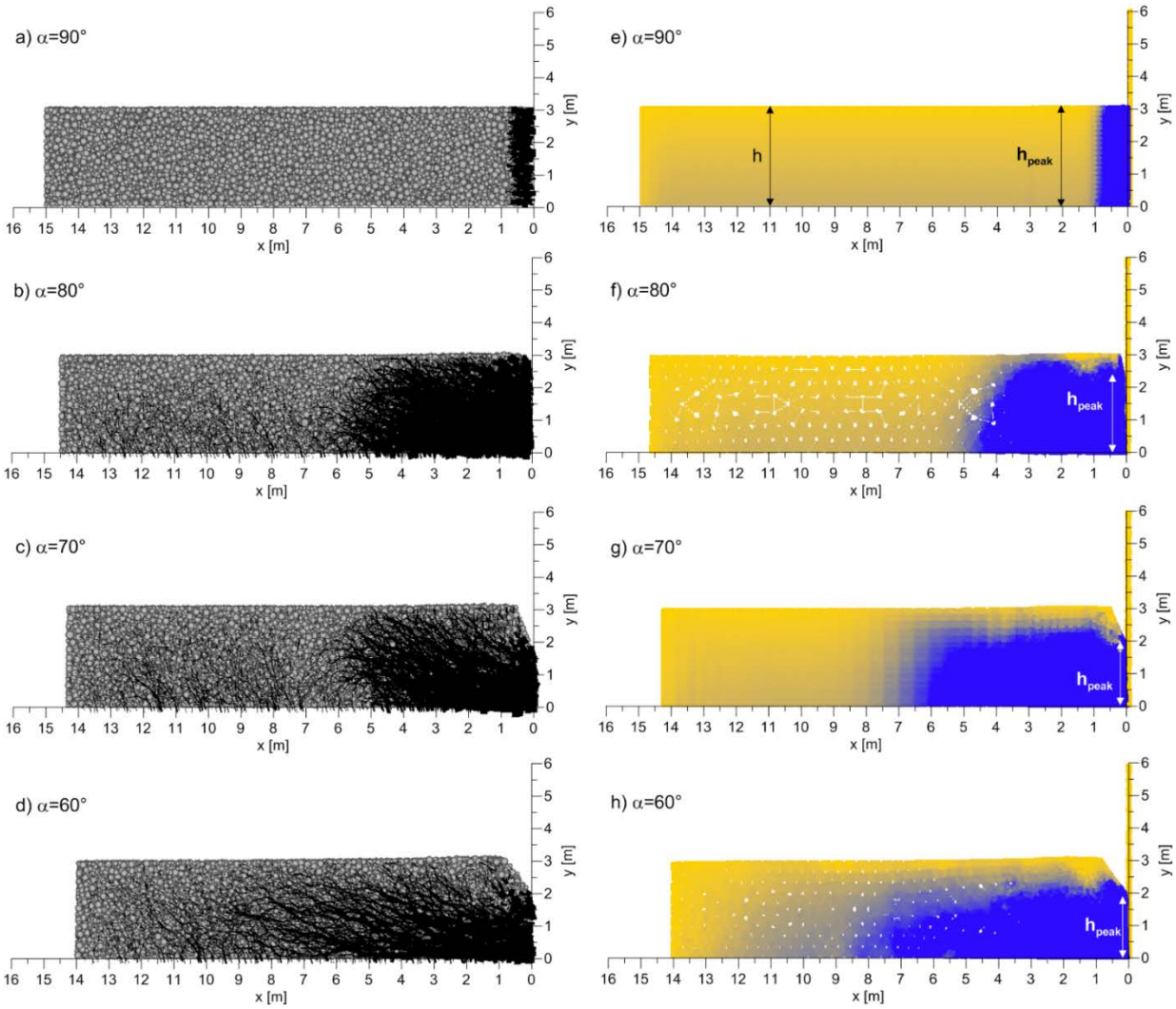

Figure 8 Force chains (a-d) and mean effective stress (e-h) at the peak time for different front inclinations.

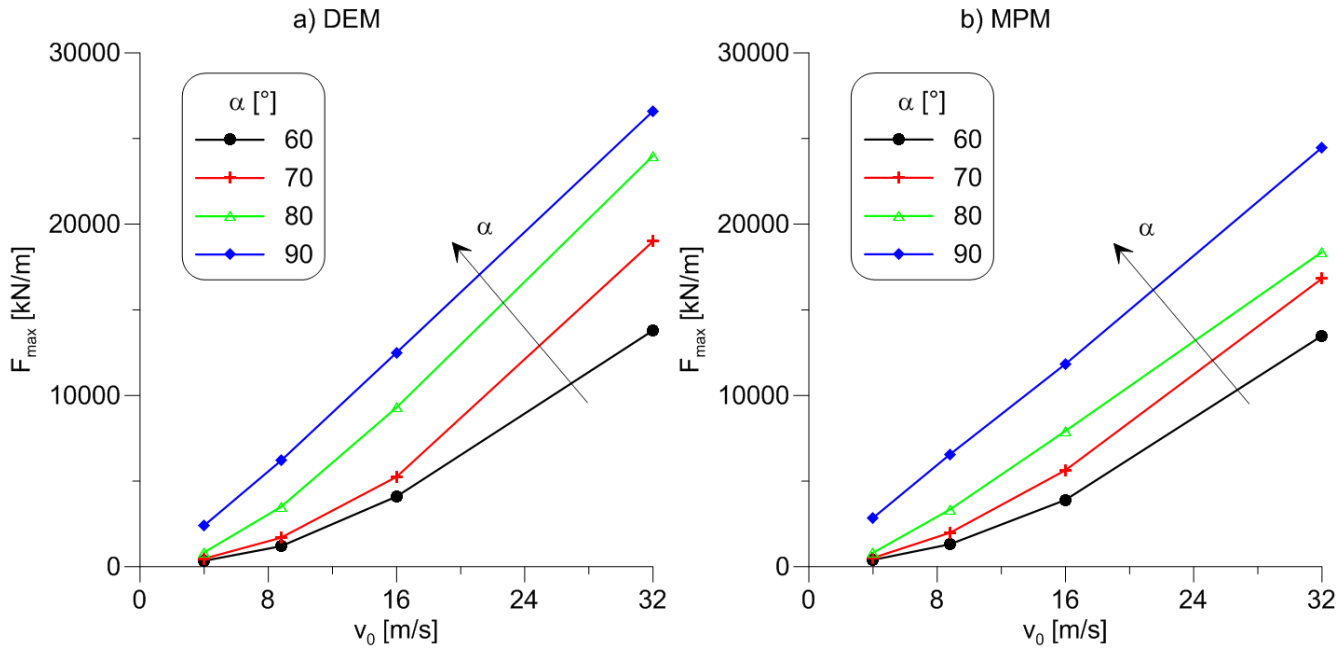

Figure 9 Maximum impact force for different impact velocities and front inclinations: DEM (a) and MPM (b) numerical results (material 1)

4.3 Effect of elastic modulus in MPM and porosity in DEM

As already mentioned in Sec. 2, the elastic modulus mainly depends on the porosity and the ratio between normal contact stiffness and grain diameter. In our parametric DEM simulations, only the porosity is varied and can be correlated to the Young modulus through the celerity of the compression wave as explained in Sec. 2.2.

In Fig. 10 the impact force evolution over time is shown for different values of porosity and Young's modulus (materials 1-5 Tab. 2) in case α=90° and v_0=8.8m/s. The agreement between the two approaches is quite satisfactory; the obtained peak forces are similar and they decrease with the Young's modulus (increasing porosity) (see Eq. 2 and 3). However, due to the dissimilar nature of the two approaches, differences are evident as well, in particular when the porosity is sufficiently high.

The DEM curves always present an initial peak, due to the impact of the first layer of particles against the wall. The higher the porosity, the lower the peak value. When the porosity is sufficiently low (i.e. n=0.45, n=0.5), force chains dominate the response of the granular medium and a large part of the energy stored due to the impact is elastic (Fig. 11a). After the peak, the impact force and the elastic stored energy decrease gradually, due to "buckling" of the contact force chains (rarefaction wave), as described previously in Sec. 3. During this phase, the energy is dissipated by the frictional force chains. In contrast, when the porosity is higher, particles cannot form stable force chains and mainly interact through inelastic collisions, which are responsible for the energy dissipation. The material can be considered as a granular liquid or gas [62–65], rather than a solid. In fact, for the

same value of the initial energy, materials with higher porosity are characterized by a larger amount of kinetic energy (Fig. 11b) and a lower amount of elastic stored energy (Fig. 11a).

In the MPM simulations, the elasto-plastic Mohr Coulomb model has been employed and the difference in porosity is simulated by using different elastic moduli, calibrated as described in Sec. 2.2, while the bulk density is constant. Therefore, to reproduce the very porous material, a very small Young modulus has been employed. In this case, the material behaves like a very compressible solid, with a constant stiffness, rather than a granular fluid or gas. When v_0>c the compression wave cannot propagate upstream and the material compacts against the wall; no peak is observed in the force evolution (Fig. 10b).

This constitutive model offers a simplified description of the material behavior; indeed, energy dissipation occurs only by internal friction and the elastic parameters are constant in space and time. However, the collisional dissipated energy and the variation of the material compressibility during impact are significant and cannot be neglected, especially in large-porosity granular flows.

In Fig. 12, the peak force is represented as function of the impact velocity for different values of n (DEM, Fig. 12a) and E (MPM, Fig. 12b). The linear dependence on v_0 is confirmed in all the considered cases; however, DEM predicts higher F_{max} for the larger values of porosity.

In Fig. 13, all the peak forces obtained with DEM and MPM for different porosities, impact velocities, and front inclinations are plotted. An excellent quantitative agreement is obtained for the lower values of porosity (n=0.45-0.50), while DEM predicts higher peak forces for n>0.5. This indicates that, with a proper selection of material parameters, the elastoplastic model can capture the behavior of low-porosity granular flows at impact (solid-like behavior). In contrast, this constitutive law is inaccurate when simulating materials having a high-porosity (liquid- or gas-like behavior). This is due to the incapability of the constitutive model to capture fundamental aspects of the granular nature of the material such as stresses and energy dissipation generated by grain collisions and modifications of the rheological behavior due to grain packing against the wall.

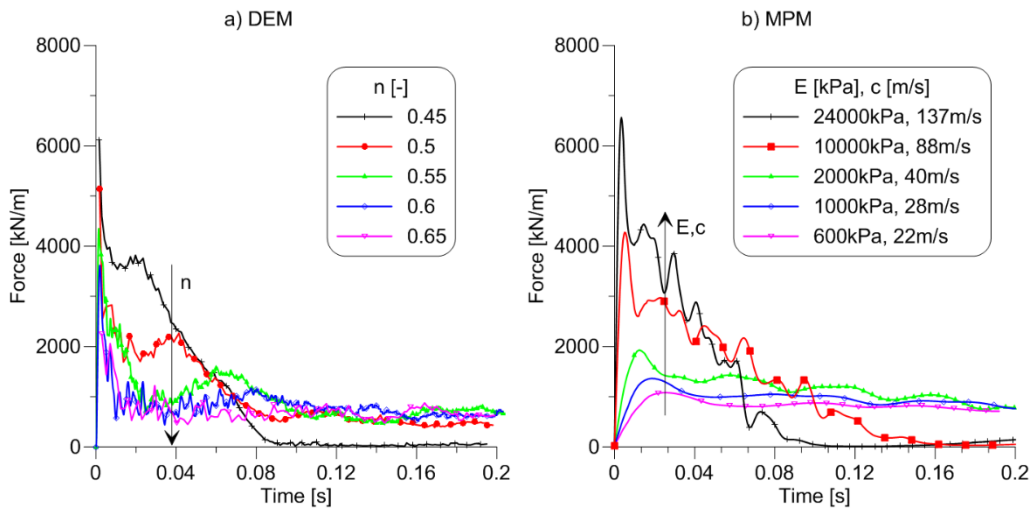

Figure 10 Impact force evolution over time for different materials: MPM (a) and DEM (b) numerical results (v_0=8.8m/s, α=90°)

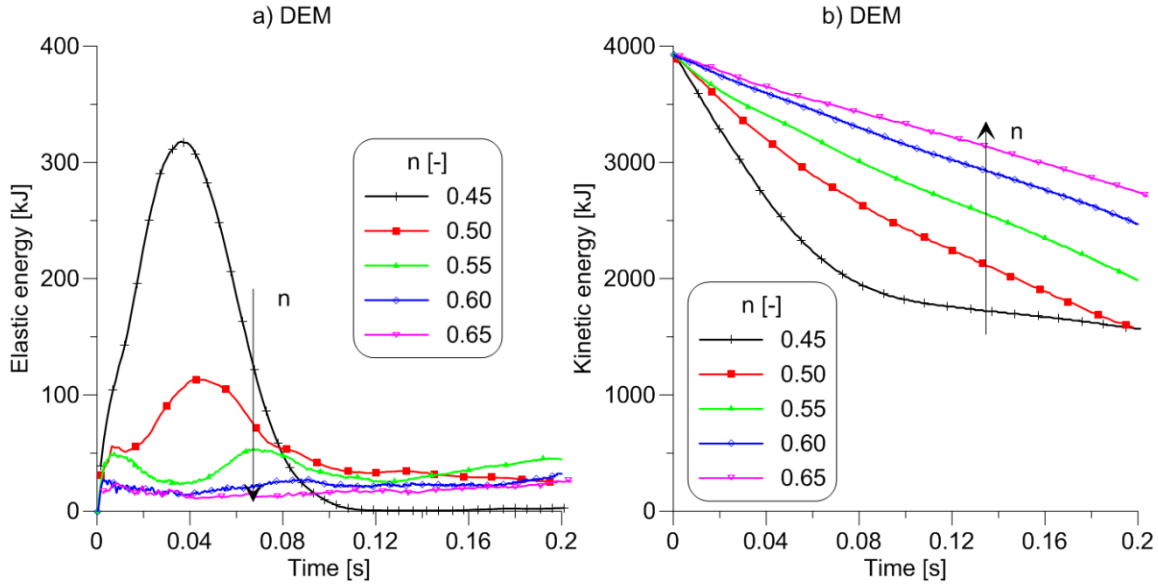

Figure 11 Evolution over time of the (a) elastic stored energy and (b) kinetic energy for different porosities for the DEM numerical simulations (v_0=8.8m/s, α=90°)

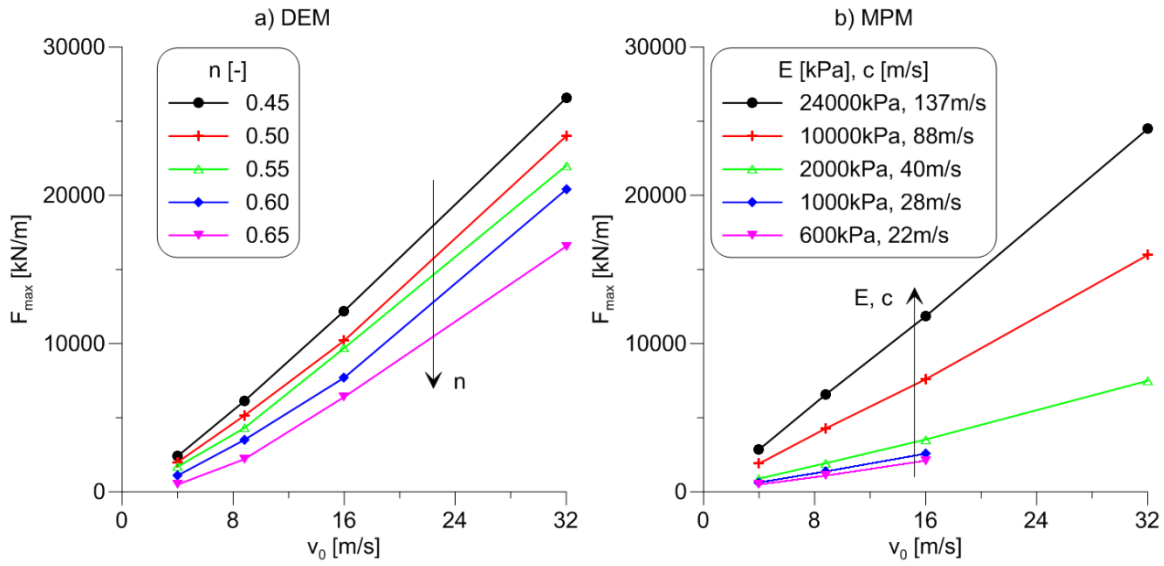

Figure 12 Maximum impact force for different impact velocities and materials: DEM (a) and MPM (b) numerical results (α=90°)

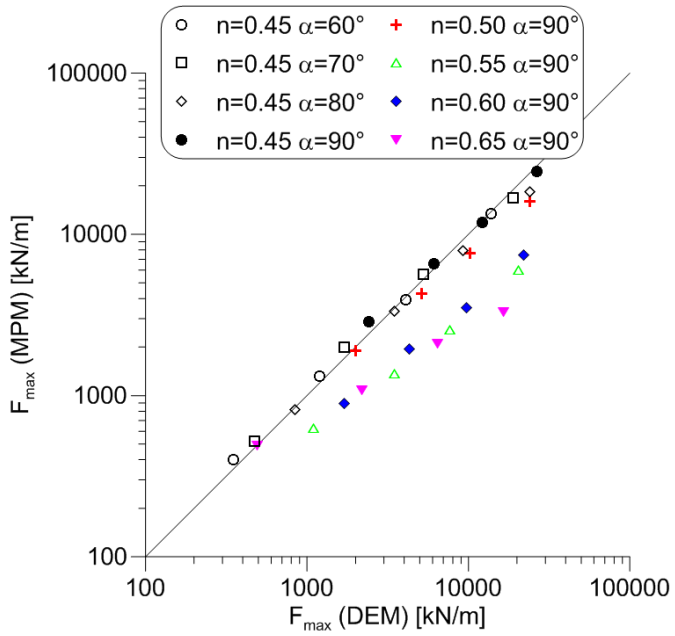

Figure 13 Peak force in DEM and MPM simulations

5 Discussion and conclusions

This paper investigates the impact process in dry granular masses comparing two different numerical approaches: a discontinuous approach based on DEM and a continuous approach based on MPM. The effects of initial porosity, velocity and front inclination have been investigated.

With discrete methods, the macroscopic behavior of the assembly derives directly from micromechanical parameters (interparticle friction angle, contact stiffness, grain characteristics) and state parameters (fabric and

porosity). The DEM model naturally takes into account the local variation of porosity and internal microstructure deriving from compaction of the material during the impact process, the dependence of the material response on packing and on strain rate, as well as the dissipation mechanisms characterizing the granular flow (frictional force chains and inelastic collisions). In contrast, in the MPM model care should be taken when choosing the constitutive model and its parameters. The adopted elastic-perfectly plastic constitutive model (Mohr-Coulomb) offers a simplistic description of the material behavior, in which the energy dissipation occurs only by internal friction and in which the elastic parameters are constant over space and time. These parameters cannot be easily correlated to the initial state of the material; in fact, the material elastic stiffness depends on the material porosity, which cannot be evaluated a priori. Therefore, the authors decided to estimate the elastic modulus from the celerity of the shock wave generated during the impact in DEM confined simulations. This strategy allows us to obtain compatible parameters between discrete and continuum methods in dynamic conditions. The proposed methodology is easy to apply in numerical simulations, but certainly difficult in a real case. Indeed, to the authors' knowledge there are no field measurements of the sound speed in rock or snow avalanches, and this parameters is often derived indirectly. Further research in this field is encouraged.

To improve the MPM results, more advanced constitutive models should be considered, possibly taking into account both frictional and collisional factors, as well as the effects of strain rate and grain packing.

Both DEM and MPM models appear to be capable of simulating the impact process and evaluating the impact force by describing its evolution over time. The agreement between the DEM and MPM numerical results is satisfactory when $n<0.5$. Both approaches capture the bi-dimensionality of the impact phenomenon dominated by compression and rarefaction waves generated at the front and the upper boundaries, respectively. The propagation of these waves, which is also influenced by the shape of the sliding mass (front inclination and height), dramatically affects the force evolution and the peak value.

In case of vertical front, the peak force increases linearly with the impact velocity and the celerity of the compression wave, which is in agreement with the theory of linear impulse. In contrast, a nonlinear F_{max}-v_0 relationship is observed in the case of inclined fronts. The impact force is strongly affected by the material porosity in the discrete approach and by the elastic parameters in the continuum approach.

In conclusion, investigating the impact process numerically can be very useful in order to better understand the physical problem. It is also relevant for practical applications, because complex geometries of the structure and different impact conditions can be considered, aiding in an optimization of the barrier design in order to reduce the costs, the environmental impact and increase the effectiveness.

Appendix A. Sensitivity analyses in DEM

In this Appendix we study the effect on DEM results of :

- Average grain diameter D;
- Friction angle of the sliding base (φ_b) and friction angle of the wall (φ_w);
- Interparticle friction angle φ_s;
- Particle rotation;

The sensitivity analyses presented in this Appendix are obtained by imposing an initial velocity v_0= 8.8m/s, a porosity n=0.45 and n=0.65 and a front inclination α=90°, if not otherwise specified.

In Fig. 14, force-time curves are plotted for different average grain diameters. It is possible to observe that for diameters smaller than 0.2m, the response is similar both in terms of maximum impact force and in terms of force evolution. The DEM simulations reported in this paper have been performed by employing an average particle diameter D=0.2m, which gives accurate results in a reasonable computational time.

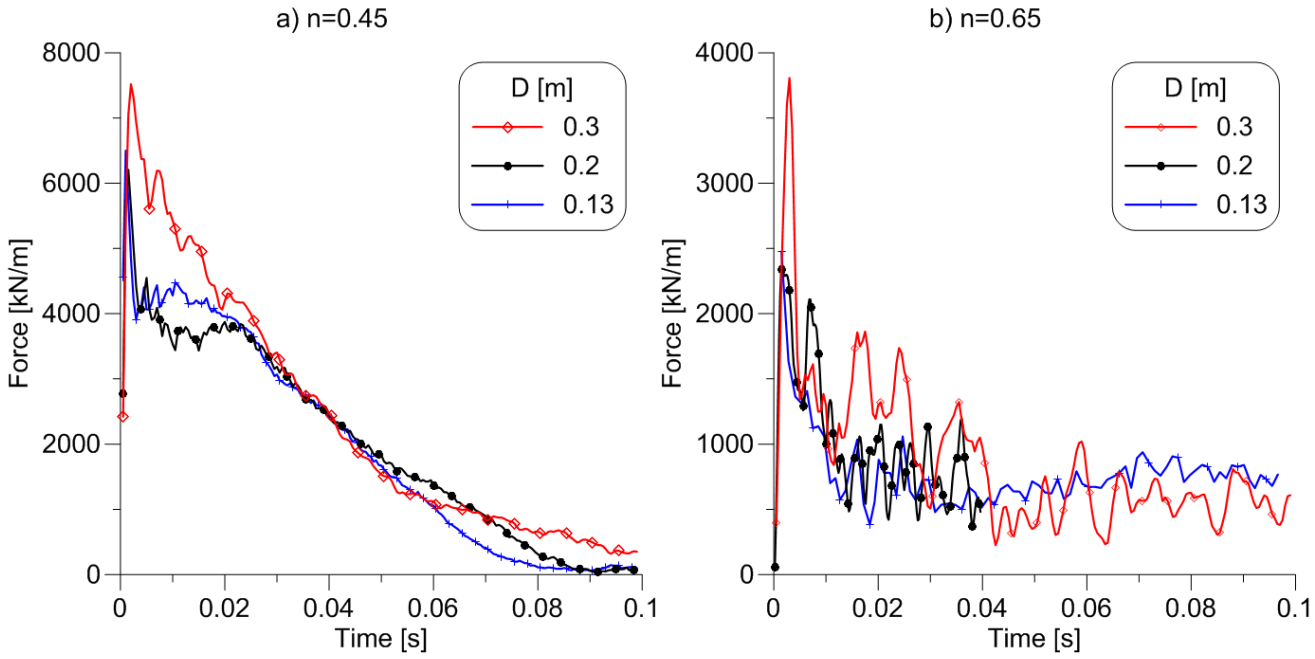

Figure 14 Evolution of the impact force over time for different values of the particle diameter and (a) n=0.45, (b) n=0.65

In case of α=90°, the basal friction angle does not affect the value of the maximum impact force, as confirmed by Fig. 15a. In fact, the maximum force develops immediately after the contact of the mass against the obstacle. Therefore, this value cannot depend on φ_b.

In case of inclined front (e.g. α=60°), the basal friction angle influences both the value of the maximum force and the time of occurrence of the peak. The higher the basal friction, the higher the energy dissipated. This is due to the fact that the maximum impact force develops later and it will depend on the energy dissipated within the soil mass and the base (this effect is magnified for smaller values of α). At the bottom of the soil mass, permanent force chains develop dissipating energy and the mass behaves like a solid; thus φ_b necessarily affects

the peak force because it modifies the energy dissipation along time. In case of both vertical and inclined front, the obstacle friction angle does not significantly affect the results. This is apparently due to the negligible effect of sliding of the mass front along the face of the obstacle.

From Fig. 16 it is evident that, if the interparticle friction is chosen in a range that is reasonable for granular geomaterials, the value of the maximum impact force remains practically the same. It is worth noting that the correlation from the value of the interparticle friction angle of Fig. 16 and the value of the macroscopic internal angle of Fig. 22 has been obtained according to Eq. 1.

In Fig. 17 the effect of particle rotation is shown. The value of the maximum impact force is the same in case of α=90° and is slightly reduced in case of α=60°.

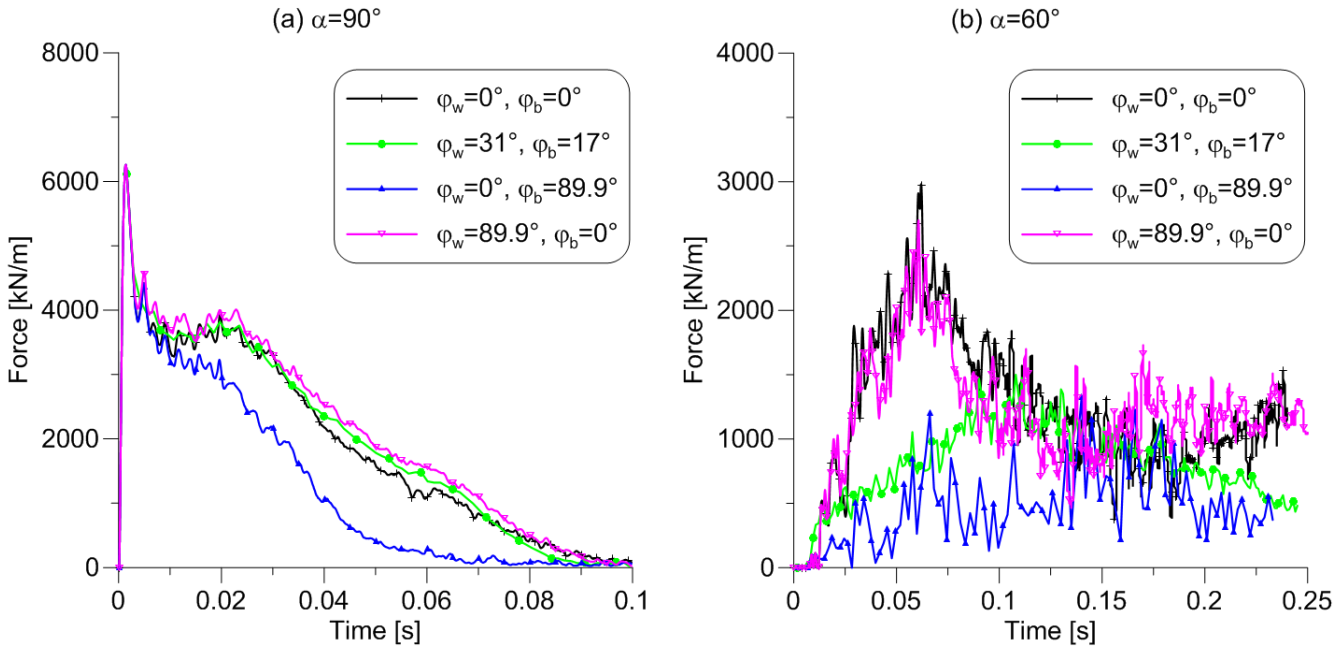

Figure 15 Effect of the basal and wall friction angle on the impact force in case (a) α=90° and (b) α=60°.

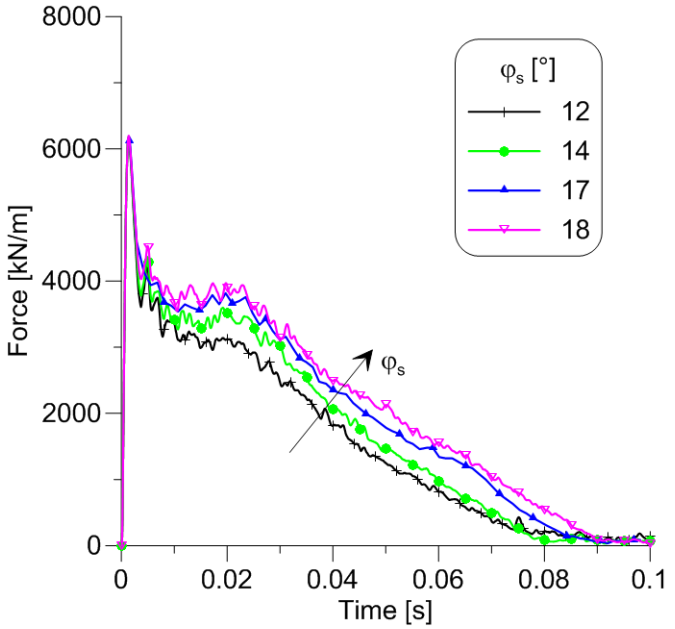

Figure 16 Effect of interparticle friction angle on the force evolution.

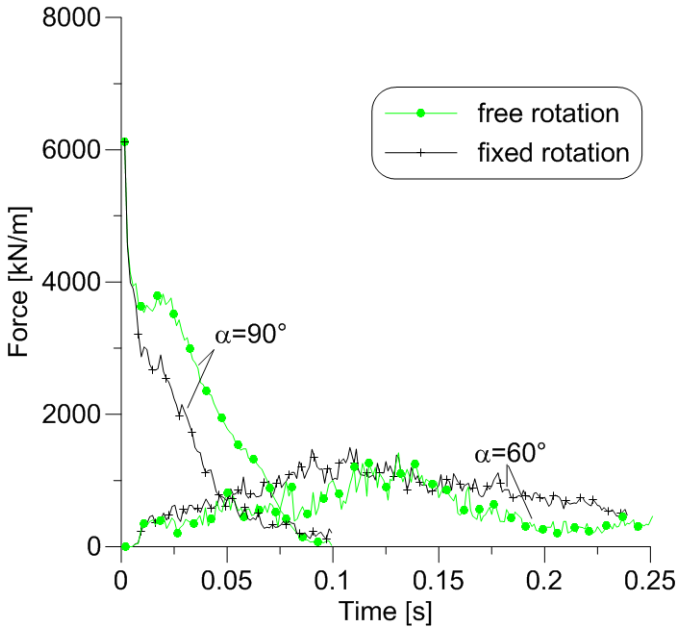

Figure 17 Effect of particle rotations on the force evolution.

Appendix B. Sensitivity analyses in MPM

In this Appendix, we discuss the effects on the results of:

- Discretization: size of finite elements and number of MP per element;
- Friction angle of the sliding base (φ_b) and friction angle of the wall (φ_w). Fully rough conditions ($\varphi_b \approx 90°$ or $\varphi_w \approx 90°$) are simulated by prescribing a fixity at the surface;
- Initial horizontal stress;

- Material soil friction angle.

The sensitivity analyses presented in this Appendix are obtained with the material properties of Material 1 (Tab. 2), impact velocity of 8.8m/s and a front inclination α=90°, if not otherwise specified. Different input parameters have also been considered and the results confirm the findings presented here.

In order to evaluate the effect of the element dimensions in MPM, we considered structured grids with different sizes of the reference prismatic unit. We considered (i) a coarse mesh characterized by 0.4m-long and 0.2m-high elements (Fig.18a), (ii) a medium-coarse mesh with 0.15m-long and 0.15m-high elements (Fig. 18b), (iii) a medium-fine mesh with 0.10m-long and 0.15m-high elements (Fig. 18c), and (iv) a fine mesh with 0.075m-long and 0.075m-high elements (Fig. 18d).

By reducing the length of the elements, the peak force is reached in a shorter time, while if the element length is too large the peak force may be underestimated (Fig. 19). The difference between the peak values measured with the medium-coarse (0.15m x 0.15m), medium-fine (0.10m x 0.10m) and fine mesh (0.075m x 0.075m) is less than 3%. The post-peak response is characterized by oscillations that have a smaller amplitude for the finer meshes, but the mean response is similar and does not affect the main findings of this study. No shock capturing strategies (e.g. bulk viscosity damping) are applied to reduce stress oscillations, which however are not very severe. Since the computational cost of the medium-fine and fine meshes is considerably higher than the one of the medium-coarse mesh, an element size of 0.15m is considered optimal for this study.

The number of material points per element does not influence the peak force and the response at the very beginning of the computation; however, higher oscillations are obtained in the following due to grid crossing errors. The movement of MP across element boundaries is known to cause stress oscillations [66,67]. In order to mitigate this problem, Gauss integration is applied in fully filled elements (elements in which the sum of the volumes of the contained MPs is greater than 90% of the element volume) [68]. This approach proved to reduce the noise significantly [40].

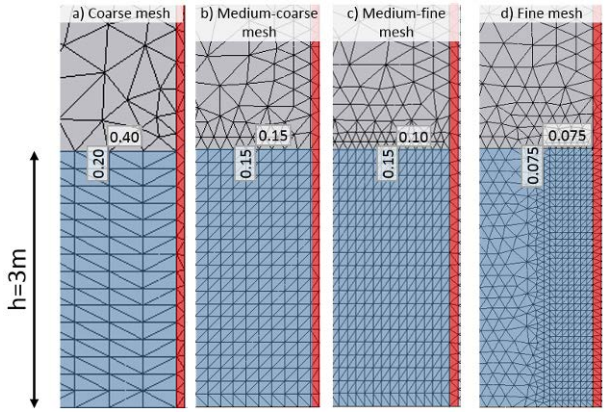

Figure 18 Discretization near the wall considered for sensitivity analyses

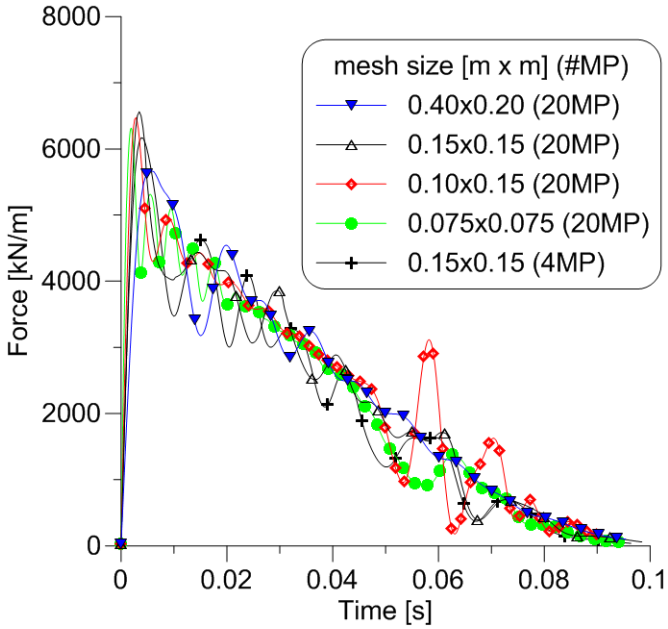

Figure 19 discretization effects in MPM

Mesh-dependency of the results is a very common drawback in many numerical methods, which should be carefully addressed especially when considering highly dynamic problems. In this study, this issue was more evident for 90°-front inclination; in contrast, a relatively small effect was observed with different front inclinations.

The basal friction coefficient is known to influence the propagation of flow-like landslides significantly [69], and thus the impact force on structures placed at the end of the flow path, because the impact velocity decreases with increasing basal friction. However, for a given impact velocity and α=90°, it does not significantly affect the peak force (Fig. 20a). In contrast, for α=60° the results change significantly because the peak is reached after a longer time and thus a larger amount of energy is dissipated by friction (Fig. 20b).

The influence of the wall friction coefficient is negligible in case of vertical wall; however, it has been shown that the roughness of the structure has an effect on the impact forces of slanted structures such as dams [69,70].

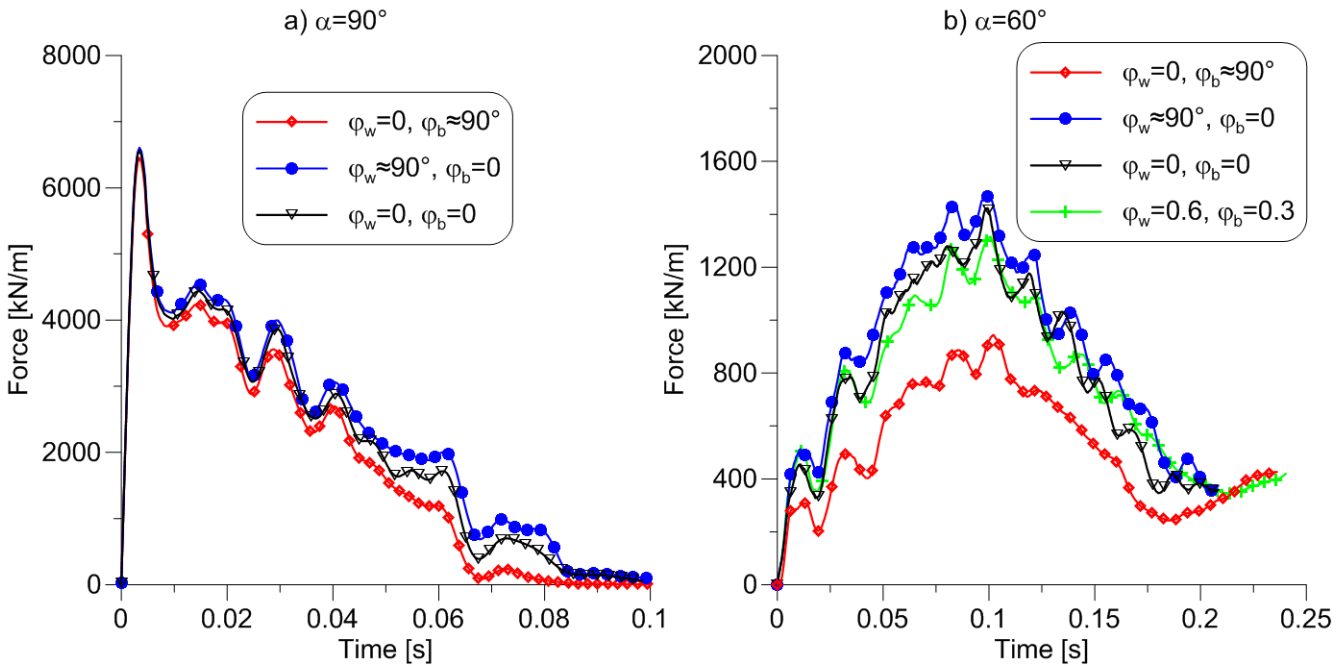

Figure 20 Effect of basal friction coefficient and wall friction coefficient on the impact forces

In this paper, initial horizontal stresses are proportional to the vertical stresses by means of a coefficient $K = 1 - \sin(\varphi)$, which corresponds to the coefficient of earth pressure at rest in normally consolidated soil. This is a strong hypothesis, thus the effect of K on the results deserves to be investigated.

Fig. 21 shows the impact force for different values of the earth pressure coefficient, where it can be seen that it has a negligible effect on the results. This is due to the fact that, in the considered range of impact velocities, the dynamic increment of the force is significantly higher than the static component.

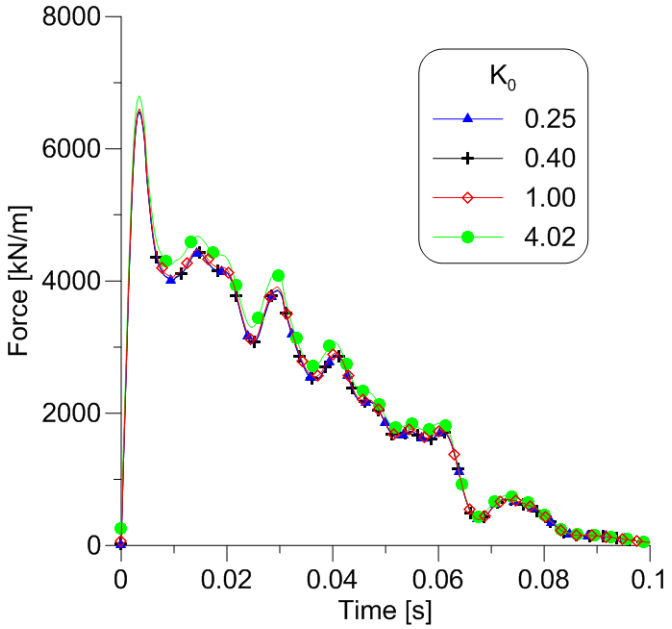

Figure 21 Effect of horizontal earth pressure coefficient on the impact force

The influence of the material friction angle on the impact force is shown in Fig. 22, where it can be seen that it does not significantly affect the peak force or the force evolution. As was already observed in case of DEM numerical results, in case of vertical front (α=90°), the peak force is not affected by the internal friction angle of the material since at that stage, when the peak force is obtained, yielding within the impacting mass has not yet diffused and it is localized close to the free surface. Considering a friction angle between 30° and 40°, the peak force varies only within 3%.

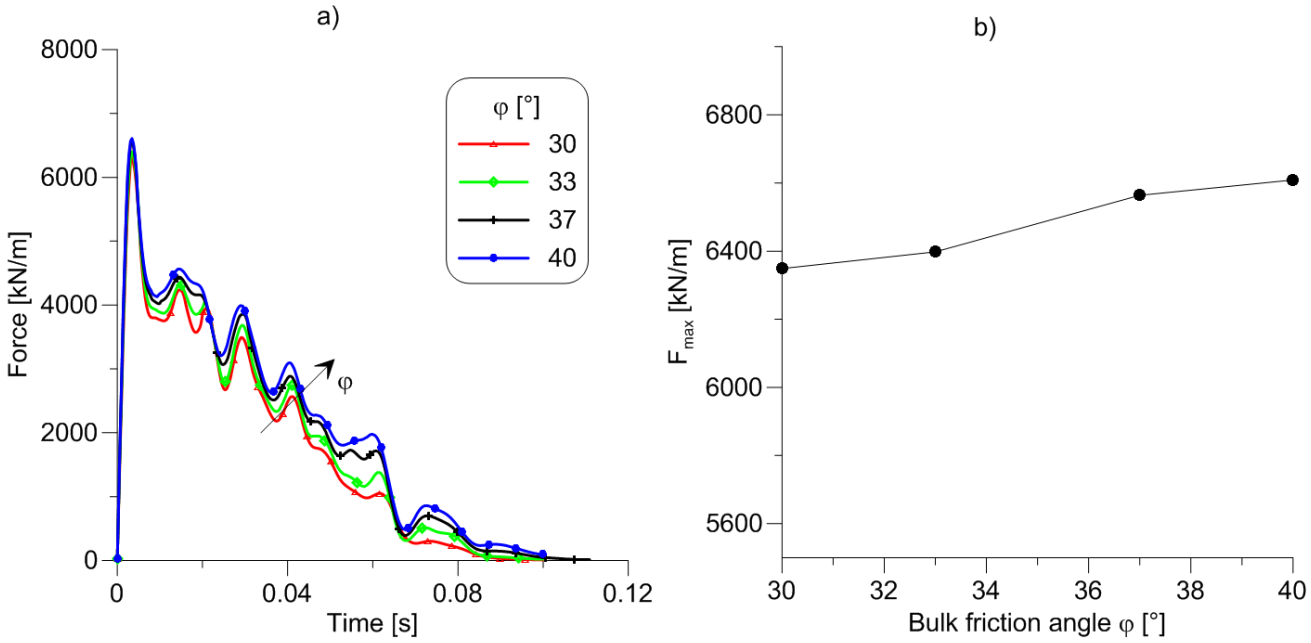

Figure 22 Effect of material friction angle on the impact force evolution (a) and its maximum value (b).

References

[1] Hungr O, Leroueil S, Picarelli L. The Varnes classification of landslide types, an update. Landslides 2014;11:167–94. doi:10.1007/s10346-013-0436-y.

[2] Armanini A. On the dynamic impact of debris flows. Recent Dev Debris Flows 1997.

[3] Scotton P, Deganutti A. Phreatic line and dynamic impact in laboratory debris flow experiments. Debris-Flow Hazards Mitig Mech Predict Assessment 1997:777–86.

[4] Bugnion L, McArdell BW, Bartelt P, Wendeler C. Measurements of hillslope debris flow impact pressure on obstacles. Landslides 2012;9:179–87. doi:10.1007/s10346-011-0294-4.

[5] Zhang S. A comprehensive approach to the observation and prevention of debris flows in China. Nat Hazards 1993.

[6] Hübl J, Suda J, Proske D, Kaitna R, Scheidl C. Debris Flow Impact Estimation. Int Symp Water Manag Hydraul Eng 2009:137–48.

[7] Arattano M, Franzi L. On the evaluation of debris flows dynamics by means of mathematical models. Nat Hazards Earth Syst Sci 2003;3:539–44. doi:10.5194/nhess-3-539-2003.

[8] Cundall P, Strack O. The development of constitutive laws for soil using the distinct element method. Numer Methods Geomech 1979:289–317.

[9] Wu JH, Chen CH. Application of DDA to simulate characteristics of the Tsaoling landslide. Comput Geotech 2011;38:741–50. doi:10.1016/j.compgeo.2011.04.003.

[10] Wu JH. Seismic landslide simulations in discontinuous deformation analysis. Comput Geotech 2010;37:594–601. doi:10.1016/j.compgeo.2010.03.007.

[11] Zorzi G, Baeßler M, Gabrieli F, Bae??ler M, Gabrieli F. Influence of Structural Stiffness on Ratcheting Convection Cells of Granular Soil under Cyclic Lateral Loading. 1st Int. Conf. Mater. Point Method, vol. 175, Elsevier B.V.; 2017, p. 148–56. doi:10.1016/j.proeng.2017.01.046.

[12] Calvetti F, di Prisco C, Vairaktaris E. DEM assessment of impact forces of dry granular masses on rigid barriers. Acta Geotech 2017;12:129–44. doi:10.1007/s11440-016-0434-z.

[13] Leonardi A, Wittel FK, Mendoza M, Herrmann HJ. Coupled DEM-LBM method for the free-surface simulation of heterogeneous suspensions. Comput Part Mech 2014;1:3–13. doi:10.1007/s40571-014-0001-z.

[14] Albaba A, Lambert S, Faug T. Dry granular avalanche impact force on a rigid wall of semi-infinite height. EPJ Web Conf 2017;140:03054. doi:10.1051/epjconf/201714003054.

[15] Wu JH, Lin WK, Hu HT. Assessing the impacts of a large slope failure using 3DEC: The Chiu-fen-erh-shan residual slope. Comput Geotech 2017;88:32–45. doi:10.1016/j.compgeo.2017.03.002.

[16] Song Y, Huang D, Zeng B. GPU-based parallel computation for discontinuous deformation analysis (DDA) method and its application to modelling earthquake-induced landslide. Comput Geotech 2017;86:80–94. doi:10.1016/j.compgeo.2017.01.001.

[17] Moriguchi S, Borja RI, Yashima A, Sawada K. Estimating the impact force generated by granular flow on a rigid obstruction. Acta Geotech 2009;4:57–71. doi:10.1007/s11440-009-0084-5.

[18] Crosta GB, Imposimato S, Roddeman D. Granular flows on erodible and non erodible inclines. Granul Matter 2015;17:667–85. doi:10.1007/s10035-015-0587-8.

[19] Crosta GB, Imposimato S, Roddeman DG. Numerical modelling of large landslides stability and runout. Nat Hazards Earth Syst Sci 2003;3:523–38. doi:10.5194/nhess-3-523-2003.

[20] Bui H, Fukagawa R. An improved SPH method for saturated soils and its application to investigate the mechanisms of embankment failure: Case of hydrostatic pore-water pressure. Int Numer Anal Methods Geomech 2013;37:31–50. doi:10.1002/nag.

[21] Idelsohn SR, Oñate E, Pin F Del, Calvo N. Fluid–structure interaction using the particle finite element method. Comput Methods Appl Mech Eng 2006;195:2100–23. doi:10.1016/j.cma.2005.02.026.

[22] Mast CM, Arduino P, Mackenzie-Helnwein P, Miller GR. Simulating granular column collapse using the Material Point Method. Acta Geotech 2014:101–16. doi:10.1007/s11440-014-0309-0.

[23] Ceccato F. Study of flow landslide impact forces on protection structures with the Material Point Method. Landslides Eng. Slopes. Exp. Theory Pract. Proc. 12th Int. Symp. Landslides, vol. 2, 2016, p. 615–20. doi:10.1201/b21520-68.

[24] Prime N, Dufour F, Darve F. Solid-fluid transition modelling in geomaterials and application to a mudflow interacting with an obstacle. Int J Numer Anal Methods Geomech 2014;38:1341–61. doi:10.1002/nag.2260.

[25] Mast CM, Arduino P, Miller GR, Mackenzie-Helnwein P. Avalanche and landslide simulation using the material point method: flow dynamics and force interaction with structures. Comput Geosci 2014:817–30. doi:10.1007/s10596-014-9428-9.

[26] Iverson R. The debris-flow rheology myth. 3rd Int Conf Debris-Flow Hazards Mitig Mech Predict Assess 2003:303–14.

[27] Ancey C. Plasticity and geophysical flows: A review. J Nonnewton Fluid Mech 2007;142:4–35. doi:10.1016/j.jnnfm.2006.05.005.

[28] Major JJ. Depositional Processes in Large-Scale Debris-Flow Experiments. J Geol 1997;105:345–66. doi:10.1086/515930.

[29] Moriguchi S, Sawada K, Uzuoka R. Numerical Simulation on Flow Failure of Geomaterials Based on Fluid Dynamics. Soils Found 2005;45:155–65.

[30] Domnik B, Pudasaini SP, Katzenbach R, Miller SA. Coupling of full two-dimensional and depth-averaged models for granular flows. J Nonnewton Fluid Mech 2013;201:56–68. doi:10.1016/j.jnnfm.2013.07.005.

[31] Bartelt P, Salm B, Gruber U. Calculating dense-snow avalanche runout using a Voellmy-fluid model with active/passive longitudinal straining. J Glaciol 1999;45.

[32] Redaelli I, di Prisco C, Vescovi D. A visco-elasto-plastic model for granular materials under simple shear conditions. Int J Numer Anal Methods Geomech 2015:n/a-n/a. doi:10.1002/nag.2391.

[33] Jiang Y, Liu M. Granular solid hydrodynamics. Granul Matter 2009;11:139–56. doi:10.1007/s10035-009-0137-3.

[34] Jop P, Forterre Y, Pouliquen O. A constitutive law for dense granular flows. Nature 2006;441:727–30. doi:10.1038/nature04801.

[35] Redaelli I, Ceccato F, Prisco CGD, Simonini P. MPM simulations of granular column collapse with a new constitutive model for the solid-fluid transition. 5th Int Conf Part Methods - Fundam Appl Part 2017 2017:539–45.

[36] Sulsky D, Chen Z, Schreyer HL. A particle method for hystory-dependent materials. Comput Methods Appl Mech Eng 1994;118:179–96.

[37] Zhou GGD, Sun QC. Three-dimensional numerical study on flow regimes of dry granular flows by DEM. Powder Technol 2013;239:115–27. doi:10.1016/j.powtec.2013.01.057.

[38] Poisel R, Prech A, Hungr O. Run Out of Landslides – Continuum Mechanics versus Discontinuum Mechanics Models. Geomech Und Tunnelbau 2008;1:358–66. doi:10.1002/geot.200800036.

[39] Teufelsbauer H, Wang Y, Pudasaini SP, Borja RI, Wu W. DEM simulation of impact force exerted by granular flow on rigid structures. Acta Geotech 2011;6:119–33. doi:10.1007/s11440-011-0140-9.

[40] Al-Kafaji IKJ. Formulation of a Dynamic Material Point Method (MPM) for Geomechanical Problems. Ph.D. thesis, University of Struttgart, Germay, 2013.

[41] Ceccato F. Study of large deformation geomechanical problems with the Material Point Method. Ph.D. thesis, University of Padua, Italy, 2014.

[42] Yerro A. MPM modelling of landslides in brittle and unsaturated soils. Ph.D thesis, Univestitat Politecnica de Catalunya, Spain, 2015.

[43] Soga K, Alonso E, Yerro A, Kumar K, Bandara S. Trends in large-deformation analysis of landslide mass movements with particular emphasis on the material point method. Géotechnique 2016;66:248–73. doi:10.1680/jgeot.15.LM.005.

[44] Yerro A, Alonso EE, Pinyol NM. Run-out of landslides in brittle soils. Comput Geotech Geotech 2016:1–13. doi:10.1016/j.compgeo.2016.03.001.

[45] Phuong NTV, van Tol AF, Elkadi ASK, Rohe A. Numerical investigation of pile installation effects in sand

using material point method. Comput Geotech 2016;73:58–71. doi:10.1016/j.compgeo.2015.11.012.

[46] Ceccato F, Beuth L, Vermeer PA, Simonini P. Two-phase Material Point Method applied to the study of cone penetration. Comput Geotech 2016;80:440–52. doi:10.1016/j.compgeo.2016.03.003.

[47] Ceccato F, Simonini P. Numerical study of partially drained penetration and pore pressure dissipation in piezocone test. Acta Geotech 2016;12:195–209. doi:10.1007/s11440-016-0448-6.

[48] Ceccato F, Bisson A, Cola S. Large displacement numerical study of 3D plate anchors Large displacement numerical study of 3D plate anchors. Eur J Environ Civ Eng 2017. doi:10.1080/19648189.2017.1408498.

[49] Bolognin M, Martinelli M, Bakker KJ, Jonkman SN. Validation of material point method for soil fluidisation analysis. 1st Int. Conf. Mater. Point Method, MPM 2017, vol. 175, Elsevier B.V.; 2017, p. 233–41. doi:10.1016/j.proeng.2017.01.018.

[50] Martinelli M, Rohe A. Modelling fluidisation and sedimentation using material point method. 1st Pan-American Congr. Comput. Mech., 2015. doi:10.13140/RG.2.1.4638.3445.

[51] Saingier G, Deboeuf S, Lagrée P-Y. On the front shape of an inertial granular flow down a rough incline. Phys Fluids 2016;28:053302. doi:10.1063/1.4948401.

[52] Leonardi A, Cabrera M, Wittel FK, Kaitna R, Mendoza M, Wu W, et al. Granular front formation in free-surface flow of concentrated suspensions. Phys Rev E 2015;052204:1–10. doi:10.1103/PhysRevE.92.052204.

[53] Ishikawa N, Inoue R, Hayashi K, Hasegawa Y, Mizuyama T. Experimental Approach on measurement of impulsive fluid force using debris flow model. Conf Proc Interpraevent 2008;1:343–54.

[54] Iverson RM. Mechanics of Debris Flows and Rock Avalanches. Handb Environ Fluid Dyn 2013:573–87.

[55] Calvetti F. Discrete modelling of granular materials and geotechnical problems. Eur J Environ Civ Eng 2008;12:951–65. doi:10.1080/19648189.2008.9693055.

[56] Itasca. PFC3D, Theory and background 2011.

[57] Bardenhagen SG, Guilkey JE, Roessig KM, Brackbill JU, Witzel WM, Foster JC. An improved contact algorithm for the material point method and application to stress propagation in granular material. C - Comput Model Eng Sci 2001;2:509–22.

[58] Anura3D Research Comunity. Anura3D MPM Software – Scientific manual 2017;1:72.

[59] Suiker ASJ, Fleck NA. Frictional Collapse of Granular Assemblies. J Appl Mech 2004;71:350. doi:10.1115/1.1753266.

[60] Johannesson T, Gauer P, Issler P, Leid K. The design of avalanche protection dams. 2009. doi:10.2777/12871.

[61] Ceccato F, Simonini P, Prisco C, Redaelli I. The effect of the front inclination on the impact forces transmitted by granular flows to rigid structures. WLF 2017 Adv. Cult. Living with Landslides, Lubiana:

2017, p. 593–9. doi:https://doi.org/10.1007/978-3-319-53498-5_69.

[62] Jaeger HM, Nagel SR, Behringer RP. Granular solids, liquids, and gases. Rev Mod Phys 1996;68:1259–73. doi:10.1103/RevModPhys.68.1259.

[63] Goldhirsch I. rapid granular flows. Annu Rev Fluid Mech 2003;35:267–93. doi:10.1146/annurev.fluid.35.101101.161114.

[64] Savage SB. The mechanics of rapid granular flows. Adv Appl Mech 1984;24:289–366.

[65] Campbell CS. Granular material flows - An overview. Powder Technol 2006;162:208–29. doi:10.1016/j.powtec.2005.12.008.

[66] Steffen M, Kirby RM, Berzins M. Analysis and reduction of quadrature errors in the material point method (MPM). Int J Numer Methods Eng 2008;76:922–9448. doi:10.1002/nme.

[67] Andersen S, Andersen L. Analysis of spatial interpolation in the material-point method. Comput Struct 2010;88:506–18. doi:10.1016/j.compstruc.2010.01.004.

[68] Beuth L, Wiecowski Z, Vermeer PA. Solution of quasi-static large-strain problems by the material point method. Int J Numer Anal Methods Geomech 2011;35:1451–65. doi:10.1002/nag.

[69] Ceccato F, Simonini P. Study of landslide run-out and impact on protection structures with the Material Point Method. INTERPRAEVENT 2016 - Conf. Proc., Lucerne: 2016.

[70] Ceccato F, Simonini P. Numerical based design of protection systems agains landslides. Work Numer Methods Geotech 2017:239–56.